EARTHQUAKE SPECTRA

The Professional Journal of the Earthquake Engineering Research Institute

PREPRINT

This preprint is a PDF of a manuscript that has been accepted for publication in *Earthquake Spectra*. It is the final version that was uploaded and approved by the author(s). While the paper has been through the usual rigorous peer review process for the Journal, it has not been copyedited, nor have the figures and tables been modified for final publication. Please also note that the paper may refer to online Appendices that are not yet available.

We have posted this preliminary version of the manuscript online in the interest of making the scientific findings available for distribution and citation as quickly as possible following acceptance. However, readers should be aware that the final, published version will look different from this version and may also have some differences in content.

The DOI for this manuscript and the correct format for citing the paper are given at the top of the online (html) abstract.

Once the final, published version of this paper is posted online, it will replace the preliminary version at the specified DOI.

Fragility based methodology for evaluating the time-dependent seismic performance of post-tensioned timber frames

Gabriele Granello[a], Marco Broccardo[b], Alessandro Palermo[c] and Stefano Pampanin[d].

Since 2010, the construction of post-tensioned wooden buildings (Pres-Lam) has been growing rapidly worldwide. Pres-Lam technology combines unbonded post-tensioning tendons and supplemental damping devices to provide moment capacity to beam-column, wall-foundation or column-foundation connections. In low seismic areas, designers may choose not to provide additional damping, relying only on the post-tensioning contribution. However, post-tensioning decreases over time due to creep phenomena arising in compressed timber members. As a consequence, there is a reduction of the clamping forces between the elements. This reduction affects the seismic response of Pres-Lam buildings in the case of low and high-intensity earthquakes.

Therefore, understanding and accounting for the post-tensioning losses and their uncertainty are paramount for a robust assessment of the safety of Pres-Lam constructions. So far, however, there have been no comprehensive studies which tackle the overall seismic performance of such systems in the presence of time-varying post tension losses and the associated uncertainty. This study tackles this research gap by introducing a comprehensive seismic evaluation of Pres-Lam systems based on time-dependent fragility curves. The proposed fragility analysis is specifically designed to account systematically for time-varying post tension losses and the related uncertainty.

The method is applied to two case studies, designed respectively with and without supplemental damping devices. In terms of structural performance, results show that the use of additional dissipaters mitigates the effect of post-tensioning loss for

[a] Lecturer, Department of Civil Engineering, University of Canterbury, New Zealand
[b] Senior Researcher, Swiss Seismological Service, and Lecturer, Department of Civil Engineering, ETH Zurich, Zurich.
[c] Professor, Department of Civil Engineering, University of Canterbury, New Zealand
[d] Professor, Department of Structural and Geotechnical Engineering, Sapienza University of Rome, Italy

earthquakes of high intensity. Conversely, performance under low-intensity earthquakes is strongly dependent on the post-tensioning value, as the reduction of stiffness due to the anticipated rocking motion activation would lead to damage to non-structural elements.

INTRODUCTION

In the 1990s, the Precast Seismic Structural System (PRESSS) program (Priestley, 1991) showed that the hybrid connection is an efficient low-damage solution for precast concrete walls and frames. The hybrid connection combines unbonded post-tensioning tendons and additional dissipation devices or internal reinforcement. The key idea is to absorb the seismic demand through a rocking mechanism between structural elements.

Specifically, unbonded tendons provide re-centering capabilities to the building, and dissipation devices allow hysteretic energy release as well as additional moment capacity. These damping devices can be placed internally by de-bonding mild steel reinforcement bars, (e.g., Curtain et al., 2012), or externally (e.g., Marriott et al., 2009; Sarti et al., 2016) to the connection. In this last case, they have the additional advantage of being easily accessible for replacement.

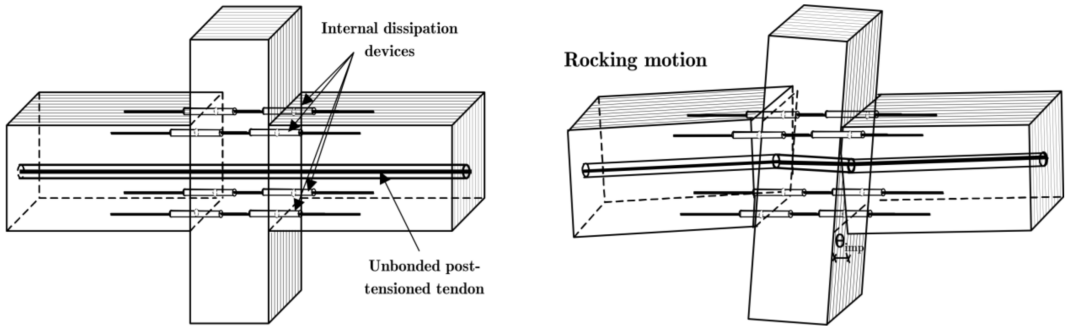

Figure 1. Post-tensioned timber beam-column connection (modified from Paerlmo et al., 2005).

In 2002, Christopoulos et al. (2002) extended the hybrid concept to steel members, supporting the idea that the hybrid connection is material independent. Following this line of thought, in 2005, the technology was extended to engineered timber products (Figure 1) also known as the Pres-Lam system (Palermo et al., 2005).

Extensive laboratory testing (e.g., Newcombe et al., 2008; Wanninger and Frangi, 2014; Sarti et al., 2015; Moroder et al., 2018) showed that the post-tensioned timber connection has

remarkable seismic performance: in fact, it presents negligible residual displacements, negligible structural damage in the timber members, and stable non-degrading hysteretic response. Furthermore, analytical and numerical models (e.g., Smith et al., 2014; Ponzo et al., 2017) were developed to capture the dynamic response of such structures.

Following these successful testing, several post-tensioned timber buildings (Figure 5) were built around the world (e.g., Curtain et al., 2012; Brown et al., 2012; Leyder et al., 2015; Holden et al., 2016; Sarti et al., 2017b).

Figure 2. Examples of operative Pres-Lam structures and beam-column joint detailing: a) Trimble Navigation Offices, Christchurch (courtesy of Paul Drummond) using b) external steel plates in the beam column joint; c) ETH House of Natural Resources, Zurich (copyright ETH Zurich-Marco Carocari) using d) hardwood columns (copyright ETH Zurich-Marco Carocari); e) Merritt Building, Christchurch (courtesy of Andy Buchanan) using f) internal steel plates (courtesy of Andy Buchanan).

This large body of research has extensively investigated the seismic performance of Pres-Lam structures; however, the long-term performance of such systems is still an open research topic. Post-tensioning decreases over time because of creep phenomena arising in compressed timber members. This causes a reduction of the clamping forces between the structural element and a potential increment of the seismic vulnerability.

Few experimental results are currently available regarding the post-tensioning loss over time expected in a post-tensioned timber system. Davies and Fragiacomo (2011) monitored post-tensioned beam and frames specimens in both controlled and uncontrolled environmental conditions for approximately 12 months. They recorded a post-tensioned loss equal to 9% for the frames, while the post-tensioning loss was found equal to 1.4% for the beams. The reason for such discrepancy was found to be the amount of timber loaded perpendicular to the grain. The authors also provided analytical creep functions for the New Zealand Laminated Veneer Lumber (LVL) Radiata Pine.

Wanninger et al. (2014) tested post-tensioned Glue Laminated Timber (Glulam) beam-column joints and post-tensioned beams for approximately 18 months. Post-tensioning losses were recorded up to 11% in the joint specimens, while they were recorded equal to 2% in the beams. The authors also provided the analytical creep functions for Swiss ash and spruce Glulam.

Building up on the analytical model proposed by Fragiacomo and Davies (2011), as well as on the experimental creep functions obtained by Davies and Fragiacomo (2011) and Wanninger et al. (2014), a design procedure to estimate the amount of post-tensioning losses in post-tensioned timber systems was proposed by Granello et al. (2018a). This procedure is adopted in this study to describe the mean value of post-tensioning over time.

Since the creep functions were calibrated over 1 or 2 years of experimental data, which is rather a small amount of time compared to a typical building service life, uncertainty is not negligible in the post-tensioning prediction. Furthermore, creep material properties are subjected to internal variability, and therefore they affect the accuracy of the post-tensioning prediction. Granello et al. (2018b) conducted a preliminary study to evaluate the impact of the variability of post-tensioning losses scenarios on the seismic performance of Pres-Lam frames. Results showed that dissipaters, if provided, are able to mitigate the effect of post-tensioning losses on the interstorey drift demand when high seismic events occur. However, being the the post-tensioning loss development over time subjected to large uncertainty, a more refined

probabilistic approach is necessary to properly estimate the in time seismic performance of such structures.

Therefore, this study represents the first attempt to develop a holistic strategy for quantifying the lifetime seismic performance of post-tensioned timber structures in the presence of input and post-tension loss uncertainty.

The proposed methodology is based on the well-known concept of fragility analysis; (Shinozuka et al., 2000; Baker, 2015) however, in this study, the parameters of the fragility curves are considered as time-varying stochastic processes. This allows a consistent integration of the post-tensioning loss and the related uncertainty.

The structure of this paper is as follows. In the first part, both the analytical and probabilistic formulation are presented. Specifically, the first section defines a probabilistic model for estimating the amount of post-tensioning losses in post-tensioned timber systems based on the analytical model proposed by Granello et al. (2018a). The second section focuses on the definition of the time variant fragility functions. The second part of the paper focuses on two case studies. Specifically: a structure placed in high seismic zone (designed with additional damping devices), and a structure placed in low seismic zone (designed without additional damping devices) to evaluate the influence of additional dissipation devices for the whole range of seismic event scenarios. Ground motion selection and probabilistic modeling of the post-tensioned losses are reported in details.

METHODOLOGY

PROBABILISTIC MODEL FOR POST-TENSIONING LOSSES IN POST-TENSIONED TIMBER SYSTEMS

Following Granello et al. (2018a), the amount of post-tensioning over time, $\mu_{PT}(t)$, is expressed as

$$\mu_{PT}(t) = P_0 - \frac{-P_0 \left\{ \frac{l_{\parallel}\phi_{\parallel}(t)}{E_{\parallel}A_{\parallel}} + \frac{l_{\perp}\phi_{\perp}(t)}{E_{\perp}A_{\perp}} + \frac{l r_p(t)}{E_p A_p [1-\chi(t)_p r_p(t)]} \right\} + \Delta\epsilon_{\parallel,in}(t) l_{\parallel} + \Delta\epsilon_{\perp,in}(t) l_{\perp} - \Delta\epsilon_{p,in}(t) l}{\frac{l_{\parallel}[1+\chi(t)_{\parallel}\phi_{\parallel}(t)]}{E_{\parallel}A_{\parallel}} + \frac{l_{\perp}[1+\chi(t)_{\perp}\phi_{\perp}(t)]}{E_{\perp}A_{\perp}} + \frac{l}{E_p A_p [1-\chi(t)_p r_p(t)]}} \tag{1}$$

where the indices $_{\parallel,\perp}$ refer to the correspondent timber properties parallel and perpendicular to the grain, respectively. The index $_p$ instead refers to the post-tensioning steel properties; l, A, E

respectively represent the length of timber under load, the cross-sectional area and the elastic modulus; $\phi(t), r_p(t)$ represent the timber creep function and the steel relaxation function. The terms $\Delta\epsilon_{in}$ represent the inelastic deformation due to changes in environmental conditions and P_0 the initial post-tensioning force. The function $\chi(t)$ takes into account that the analytical solution is approximated by correcting the creep or relaxation function (Chiorino et al., 1984). The reader specifically interested in the post-tensioning loss calculation is redirected to (Granello et al., 2018a) for a comprehensive overview.

In Figure 3, the analytical prediction is reported against the data monitored on an operative post-tensioned timber frame building: Trimble Navigation Building (Granello et al., 2018a). Although the prediction provides a good fit when compared with the data averaged across the different frames (Figure 3a), the error (and therefore the uncertainty) with respect to each single frame increases over time (Figure 3b).

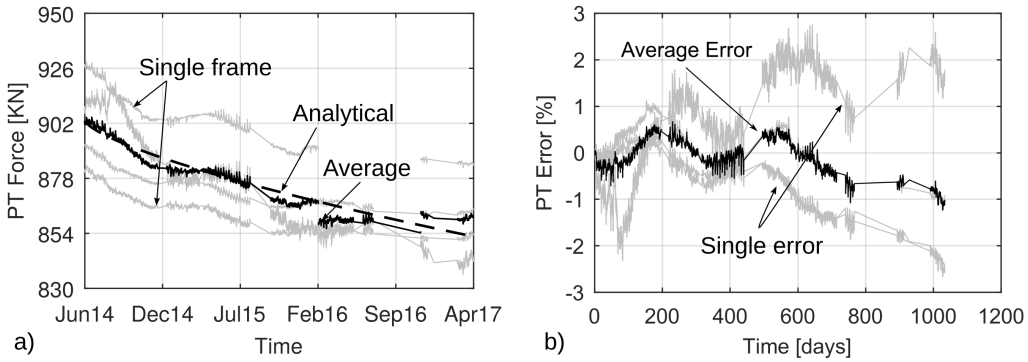

Figure 3. Comparison between analytical post-tensioning force estimation vs experimental data monitored on a post-tensioned timber building: a) post-tensioning trend and b) average error.

To capture the uncertainty evolution, the post-tensioning force, PT [a)], at the $-t$ instant can be expressed as

$$PT_t = \underbrace{\mu_{PT}(t)}_{mean\quad value} + \underbrace{\varepsilon_t}_{uncertainty}, \tag{2}$$

where $\mu_{PT}(t)$ is the mean value component, and ε_t is the random variable representing the uncertainty component.

The mean value is defined by Equation 1, and $\varepsilon_t \sim \mathcal{N}(0, \sigma_{PT}(t))$ is assumed normally distributed with zero mean and a time varying standard deviation $\sigma_{PT}(t)$. Since the uncertainty

[a)]Capital letters for PT are used only to indicate the variable "Post Tension," and not to identify a random variable. Conversely, the authors define PT_t as proper random variable defined at time t by Equation (2).

in the post-tensioning prediction is increasing exponentially over time (Granello et al., 2018a), $\sigma_{PT}(t)$ is defined as:

$$\sigma_{PT}(t) = c_1 t^{c_2}, \tag{3}$$

where c_1, c_2 are the parameters of the model.

PROBABILISTIC FORMULATION OF THE FRAGILITY FUNCTIONS

Fragility curves are defined as the probability of overcoming a specific performance level, conditional to an intensity measure, IM, (Shinozuka et al., 2000; Baker, 2015). In earthquake engineering, it is common to assume the lognormal distribution to define the fragility function (Baker, 2015; Porter, 2015) here reported in Equation 4:

$$P(D = d|IM = im; \boldsymbol{\theta}_f) = \Phi\left(\frac{\ln(im/\alpha)}{\beta}\right), \tag{4}$$

where $\Phi(\cdot)$ is the standard normal cumulative distribution function. The parameters $\boldsymbol{\theta}_f = [\alpha, \beta]$ are respectively the median α and the standard deviation β of the fragility function. The quantity IM represents the intensity measure of the seismic excitation, which was selected to be the spectral acceleration. The quantity D represents the performance level, which will be exhaustively discussed in the following section.

Since the performance of post-tensioned structures depend on the amount of post-tensioning, the parameters of the fragility functions are considered dependent on the post-tensioning level PT_t. Specifically, $A_t = \alpha(PT_t)$ and $B_t = \beta(PT_t)$. Since the post-tensioning force is a random variable which depend on the time (i.e., a stochastic process), it follows that also A_t and B_t are time-dependent random variables (i.e. stochastic processes). In the following Section we report the definition of the performance levels, D, while the expression for A_t and B_t are given for the two case studies in the second part of the paper.

PERFORMANCE LEVELS

Following the logic of FEMA P650 (2009), the performance of post-tensioned timber structures, D (Equation 4), is defined by specific indicators. In this study, two sets of indicators are used: (i) performance levels in terms of materials strain limit; and (ii) performance levels in terms of interstorey drift.

The first set of indicators aims to define suitable performance levels based on the damage

of dissipaters and on the stress-strain relationship of timber and steel at the rocking interface. Specifically, five performance levels are defined as follow:

- $PL1_{y,ms}$ corresponds to the yielding of the dissipater;
- $PL2_{u,ms}$ corresponds to the rupture of the dissipater (i.e., assumed occurring at 6% axial deformation,Priestley 2000);
- $PL3_{y,t}$ corresponds to the yielding of timber in correspondence the rocking interface;
- $PL4_{y,p}$ corresponds to the yielding of of the tendon;
- $PL5_{u,p}$ corresponds to the rupture of of the tendon.

$PL1_{y,ms}$ and $PL2_{u,ms}$ can be classified as serviceability damage state (SLS) because the damage is localized in dissipaters (i.e., it might be necessary to replace them). Conversely, $PL3_{u,t}$ and $PL4_{y,p}$ can be considered as ultimate limit states (ULS) because the structural members are permanently damaged or major repairs are necessary. Finally, $PL5_{u,p}$ is considered as collapse limit state because the system fails.

Following the philosophy of most of the building codes (e.g., New Zealand Standard, 2004; FEMA P650, 2009; Eurocode 8, 2005), the second set of indicators defines performance levels in terms of interstorey drift. Such classification assesses the whole building performance rather than focusing on the material strain in critical locations. Specifically, four performance levels are defined as follow:

- $PL1_{dr}$ corresponds to the 0.33% of the interstorey drift. According to the New Zealand Standard 1170.0 (2002), this is the drift limit for which no damage is expected in the no-structural elements (Figure 4a).
- $PL2_{dr}$ corresponds to the 2.5% of the interstorey drift. According to the New Zealand Standard 1170.5 (2004), at this level of drift, the main structural elements are subjected to damage, but the whole structure has some capacity left before collapse. It follow that this performance level is defined as a controlled damage limit state (Figure 4b).
- $PL3_{dr}$ corresponds to the 6% of the interstorey drift. At this drift level, structural collapse is expected (Figure 4c)

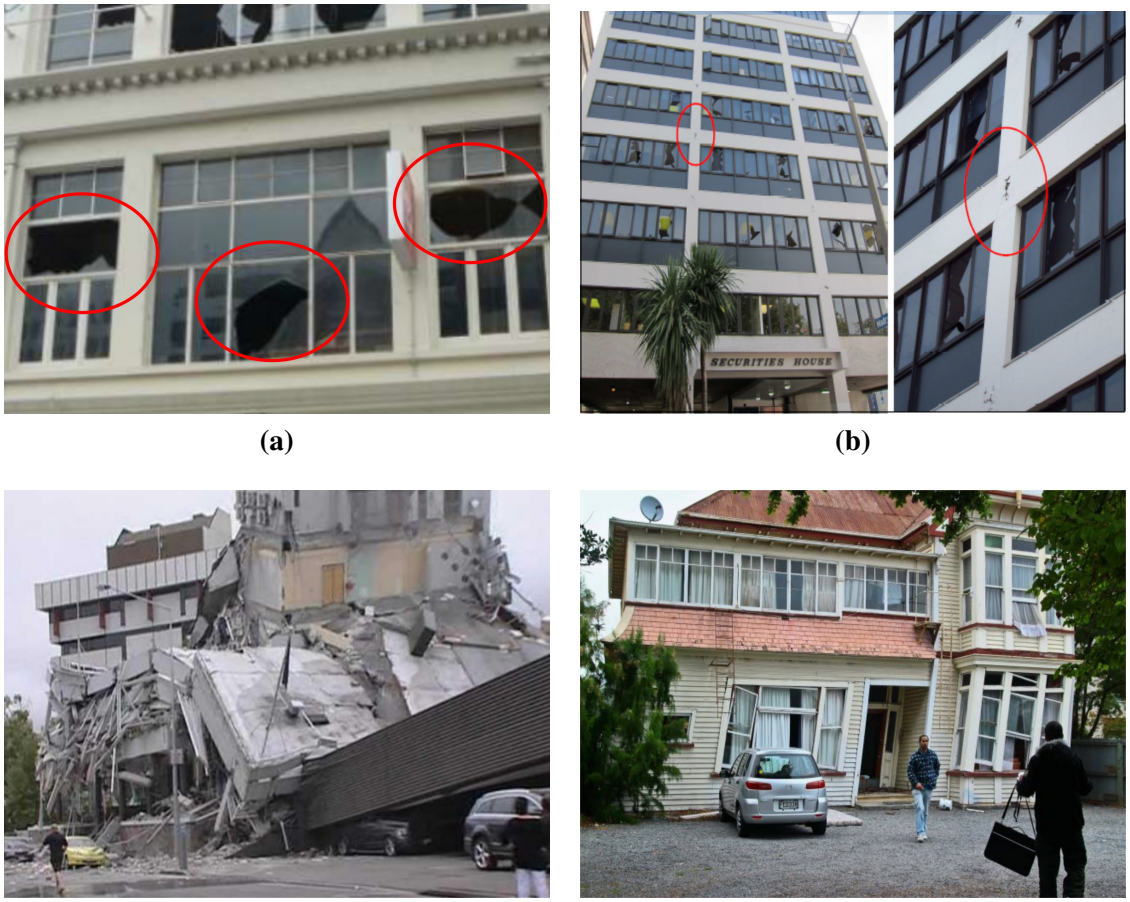

Figure 4. Performance levels: A) $PL1_{dr}$, expected damage to no structural elements (courtesy of Stefano Pampanin) ; B) $PL2_{dr}$, expected damage to structural elements (courtesy of Stefano Pampanin) C) $PL3_{dr}$, expected significant damage or collapse (source: www.tvnz.co.nz); D) $PL4_{dr}$, expected residual deformation after the seismic event (photo taken by Asher Trafford, source https://keithwoodford.wordpress.com/2011/02/27/understanding-the-christchurch-earthquake-building-damage).

- $PL4_{dr}$ corresponds to a residual interstorey drift post earthquake greater than 0.5%. This performance level is introduced to assess the re- occupancy of the building after the earthquake. In fact, according to several studies (e.g., McCormick et al. 2008; Hare et al. 2012), if the residual drift after the earthquake is greater than 0.5%, the building is likely to be demolished due to uneconomical repairs (Figure 4d).

Given these two sets of indicators, a holistic performance assessment framework for Pres-Lam structures is defined by combining performance levels of the first set with performance levels of the second set as follow:

1. The serviceability limit state 1, SLS 1, is defined as follow:

$$PL_{1,a} := PL1_{y,ms} \cup \{\text{0.5-0.7\% strain deformation}\}, \tag{5}$$

that is $PL_{1,a}$ is reached if $PL1_{y,ms}$ occurs, i.e., dissipaters are subjected to yielding[b)] *or* if the strain deformation is moderate, i.e., within 0.5-0.7%.

2. The serviceability limit state 2, SLS 2, is defined as follow:

$$PL_{1,b} := PL2_{u,ms} \cup PL1_{dr}, \tag{6}$$

that is $PL_{1,b}$ is reached if $PL2_{u,ms}$ *or* $PL1_{dr}$ occurs. In other words, this performance level occurs if the dissipaters have to be replaced at the end of the seismic event (because they are broken), or damage is expected in the non-structural elements.

3. The ultimate limit state, ULS, or controlled damage is defined as follow:

$$PL_2 := PL3_{y,t} \cup PL2_{dr}, \tag{7}$$

that is PL_2 is reached if $PL3_{y,t}$ *or* $PL2_{dr}$ occurs. In other words, this performance level occurs if damage is expected to occur on the main structural elements or the interstorey drift is greater than 2.5%.

4. The collapse limit state, CLS, is defined as follow:

$$PL_3 := PL4_{y,p} \cup PL5_{u,p} \cup PL3_{dr}, \tag{8}$$

that is PL_3 is reached if $PL4_{y,p}$ *or* $PL5_{u,p}$ *or* $PL3_{dr}$ occurs. In other words, this performance level occurs if the system fails or excessive interstorey drift greater than 5% is observed.

5. The reparability limit state (RLS) is defined as

$$PL_4 := PL4_{dr}, \tag{9}$$

that is PL_4 is reached if the residual drift after the earthquake is greater than 0.5%. In this case, the building restoration is considered economically unfeasible.

In the following sections, the described methodology is applied to investigate the effect of post-tension losses and associated uncertainty on the seismic performance of two case studies placed in high and low seismic zone, respectively.

[b)] In this case, the dissipaters can be replaced after the event at moderate cost (if external), or they can be left installed

CASE STUDY BUILDINGS

DESIGN

Two case study buildings are designed to be placed in a low (i.e., corresponding to maximum spectral acceleration in correspondence of the plateau equal to 0.54 g for a 500 years return event) and high (i.e., corresponding to a maximum spectral acceleration in correspondence of the plateau equal to 0.9 g for a 500 years return event) seismic risk area, respectively. While the first building is only post-tensioned, the second one is designed with dissipation devices at the beam-column rocking interface. Both structures are designed to be located on type D soil (New Zealand Standard 1170.5, 2004), corresponding to a deep or soft soil site.

The buildings proposed are a further development of the case study specimen (Figure 5) presented in the New Zealand and Australian Guideline for post-tensioned timber buildings (Pampanin et al., 2013). The structural systems used in that specific case-study were Pres-Lam frames in the transverse direction, and Pres-Lam walls in the longitudinal direction. This paper focuses on the seismic behavior of the frames, which are re-designed to serve as a design case study for this work.

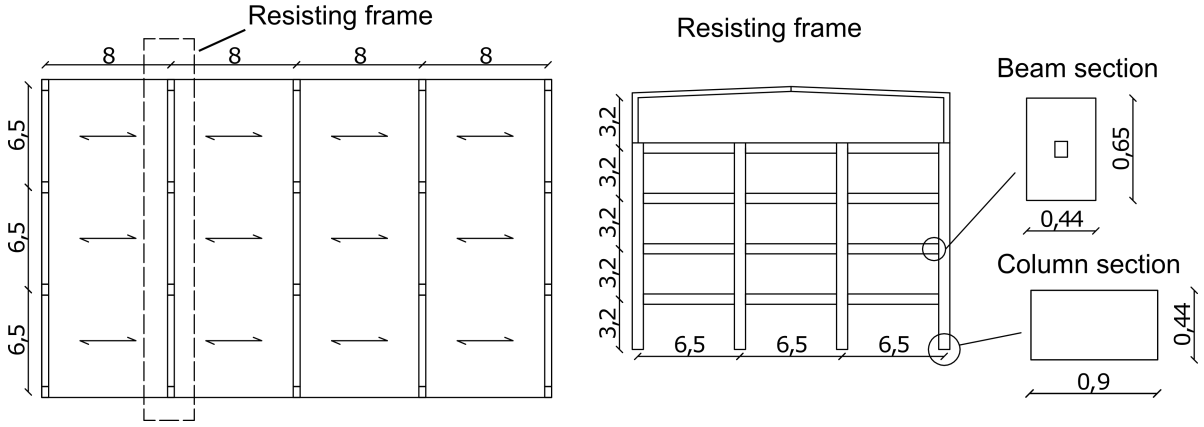

Figure 5. Plan view of the floor, lateral view of the frame and members' section (note units are in meters).

The two four-storey case study buildings are designed with a lightweight timber penthouse at the top floor. Each floor is selected to be 32 x 19.5 m in plan with a total floor area of 624 square meters (Figure 5). A building live load of 3 kPa (i.e., office use according to the New Zealand Standard 1993) is assumed to act on a floor system made up of 21 mm thick plywood panels on top of 90 x 400 mm timber joists at 0.6 m. To be consistent with the design assumptions reported in the guidelines, no concrete is placed on the top (Pampanin et al., 2013).

The design is carried out by using a displacement-based approach (Priestley et al., 2007). However, the members size and post-tensioning value are governed by the deflection limits to not be exceeded during low intensity seismic events or excessively strong winds. According to the New Zealand Standard 1170.1 (1993) , an interstorey drift equal to 0.33% should not be exceeded for an event with a return period equal to 25 years. Therefore, beam and column dimensions of 650 x 441 mm, and 900 x 441 mm respectively, are required to meet these criteria.

The timber material used for the design is LVL Radiata Pine grade 16, properties which according to the manufacturer are reported in Table 1. For the building placed in low seismic hazard, cross sections with lower dimensions could be designed to optimize the material use. However, in order to compare the results between the two cases, it has been decided to keep the same elements' size.

Table 1. LVL Grade 16 properties: f_b bending strength, $f_{c,par}$ compression strength parallel to the grain, $f_{c,perp}$ compression strength perpendicular to the grain, f_s shear strength, E_{par} elastic modulus parallel to the grain, E_{perp} elastic modulus perpendicular to the grain, G shear modulus.

f_b (MPa)	$f_{c,par}$ (MPa)	$f_{c,perp}$ (MPa)	f_s (MPa)	E_{par} (MPa)	E_{perp} (MPa)	G (MPa)
65	48	12	4.6	16	0.55	0.8

A summary of the seismic masses (considering the proper combination of dead and live loads according to the New Zealand Standard 1170.5 (2004)) is reported in Table 2.

Table 2. Seismic masses acting on the frame.

Floor	**Mass (KN)**	**Mass (KN/frame)**	**Mass (KN/wall)**
4	3130	626	782
3	3193	639	798
2	3193	639	798
1	3193	639	798
Tot	12710	2542	2542

The beam-column connection (detailed in Figure 6) with the addition of the external dissipation devices (Sarti et al., 2016), is designed to target a design re-centring ratio at the Ultmate Limit State (ULS), β_{rec}, (defined as the ratio between the post-tensioning moment contribution over the total moment capacity) of 0.7. Seven wire strands (properties reported in Table 3) are used as the post-tensioning elements. However, the number of tendons is optimized at each

for the two buildings according to the layout reported in Table 4. Ten millimetre external steel plates are designed (see Figure 6 and Figure 5b) to protect the timber in the column, which is loaded perpendicular to the grain. This solution, which was adopted in the Trimble Navigation Offices (Brown et al., 2012), also showed to have a beneficial effect in reducing the amount of post-tensioning loss expected (Granello et al., 2018a), as well as providing an anchorage point for the dissipaters.

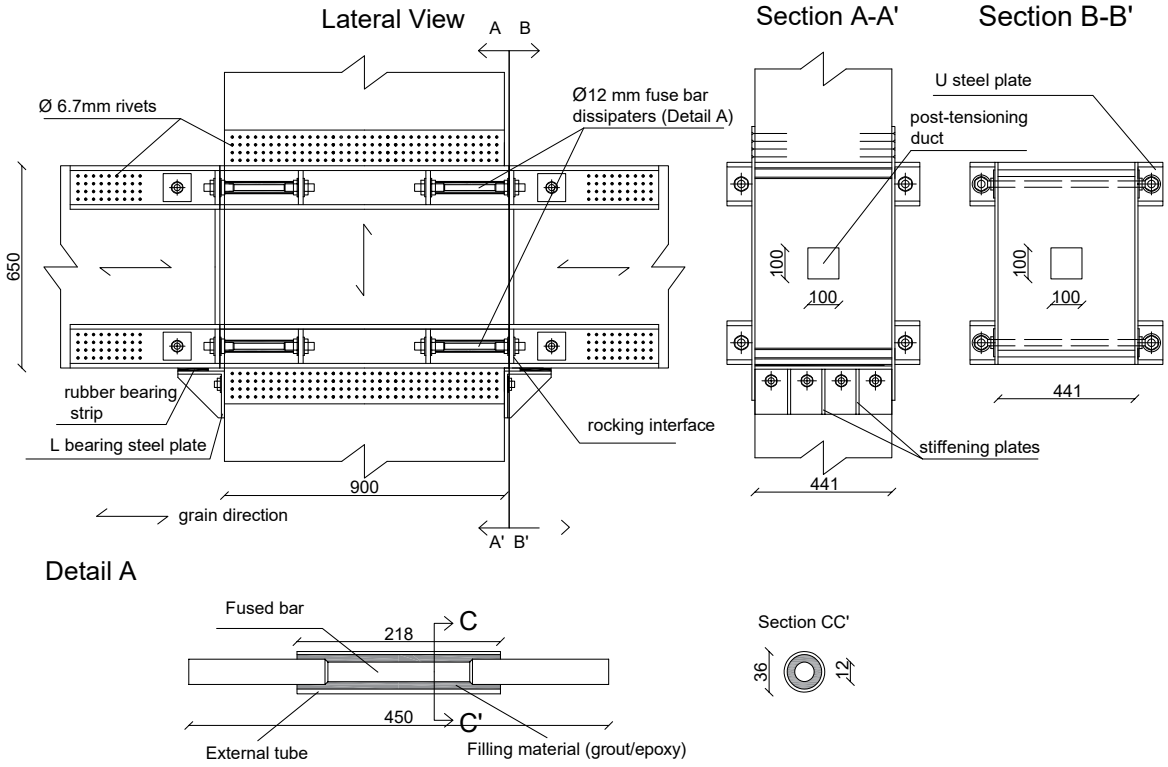

Figure 6. Structural detailing: beam-column hybrid joint and fuse dissipater.

Table 3. Steel tendon properties: Φ_i tendon diameter, A_{pi} tendon area, f_{ptk} ultimate stress, f_{pt01k} nominal yielding stress and E_p elastic modulus.

Φ_i (mm)	A_{pi} (mm^2)	f_{ptk} (MPa)	f_{pt01k} (MPa)	E_p (GPa)
12.7	100.1	1860	1674	195

While post-tensioning tendons are positioned at the section centroid of the beam section, dissipaters are placed $\pm$ 250 mm from the beam centreline (see Figure 6). The properties of the mild steel, used to fabricate the dissipaters, are reported in Table 5, while the dissipaters layout is reported in Table 4.

Table 4. Post-tensioned connection detailing with and without additional damping.

	Storey	Tendons number	Post-tensioning force (KN)	Tendons stress (% f_{pt01k})	Mild steel dissipaters
With Dissipaters	1&2	3	300	60%	4Φ12
	3&4	2	200	60%	4Φ10
Without Dissipaters	1&2	2	200	60%	-
	3&4	2	200	60%	-

Table 5. Mild steel properties respectively: f_y yielding stress, f_u ultimate stress, E_s elastic modulus, ϵ_y yielding strain, r post-yielding stiffness ration.

$f_y\ (MPa)$	$f_u\ (MPa)$	$E_s\ (MPa)$	$\epsilon_y\ (-)$	$r\ (-)$
300	420	200	0.0015	0.008

The differences between the two case study buildings are not limited to the use of dissipaters in one of the two. Specifically, a moment resisting connection (detailed in Figure 7) is designed at the column-foundation level, by introducing internal 14 mm diameter steel bars, for the building placed in high seismic area. Although the elastic period of the two case studies is almost identical, the extra moment capacity provided by the steel bars allow to increase the stiffness once the rocking motion is activated. This detailing was necessary to the interstorey drift within an acceptable value for low intensity earthquakes.

The connection between timber and steel was obtained by injecting epoxy, and the bars were de-bonded for a total length of 200 mm to distribute the plastic demand. A similar solution with the internal bars was previously adopted for the Carterton Event Centre (Curtain et al., 2012).

The possibility of introducing external dissipaters, which would be easier to replace, was also explored. However, this solution was not feasible due to the high number of connectors necessary between the dissipaters and the column. Shear keys are also provided for transferring shear, and therefore avoiding the internal bars working in dowel action.

MODELLING APPROACH

The moment-rotation behavior of a post-tensioned rocking connection was defined using an iterative analytical procedure developed by Pampanin et al. (2001), modified by Palermo et al. (2004), extended to the Pres-lam system by Newcombe et al. (2008), and further developed by Smith (2014). Such moment-rotation laws are implemented in the literature on lumped

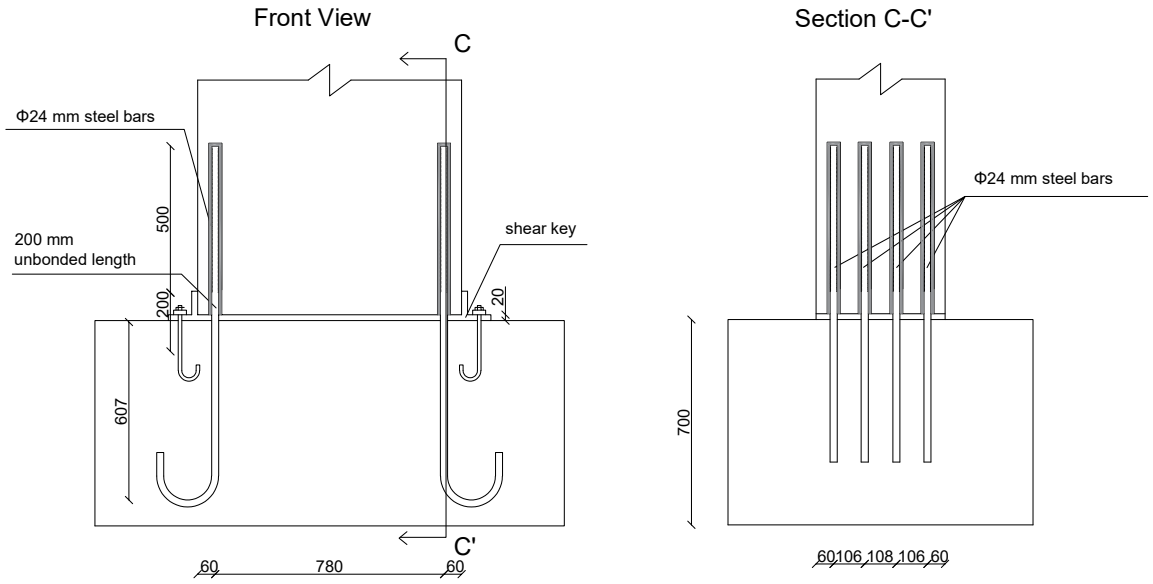

Figure 7. Column-to-foundation structural detailing.

plasticity models, using multi-spring elements (Sarti et al., 2017a), or rotational spring elements (Ponzo et al., 2017).

The difference between the two models is the ability of the multi-spring model to capture the increase of axial force in the system due to the beam elongation phenomenon. Given the large inertia of the member, this phenomenon is rather important when looking at the behaviour of post-tensioned walls (Sarti et al., 2015). However, in the case of post-tensioned frames, models based on rotational springs were shown to adequately (up to acceptable errors) predict the behavior of post-tensioned timber specimens when compared to experimental testing (Di Cesare et al., 2017).

In this work, lumped plasticity models (see Figure 8) were calibrated against the moment-rotation response by using rotational springs in parallel and in series. Specifically, (i) a multi-linear elastic hysteresis for the post-tensioning contribution, (ii) an elasto-plastic rule for the mild steel contribution, and (iii) an elastic-rigid rule for the internal rotation before the gap opening contribution. An additional rotational spring was placed at the beam-column joint to take into account the joint shear stiffness, as recommended by Smith (2014). Besides the

joints (including the column-to-foundations one), all the other elements are modeled as elastic members.

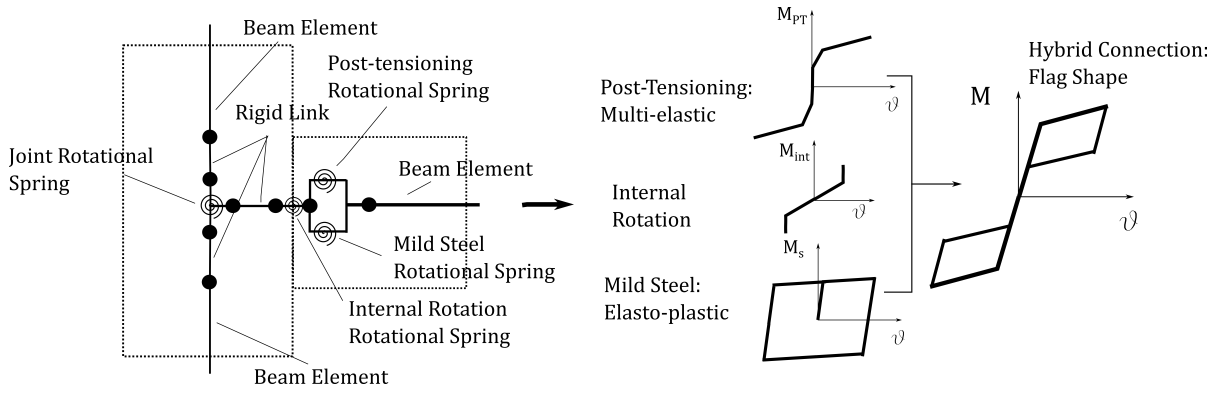

Figure 8. Post-tensioned timber connection modelling.

POST-TENSIONING LOSS ESTIMATION

It is assumed that the timber elements are delivered on site with an average moisture content equal to 12%, which is the value commonly provided by the manufacturer. It is also assumed that the environmental temperature at the time of pre-stressing is equal to $10°C$. Both these factors affect the post-tensioning trend over time: the moisture content variation affects the creep behaviour of timber, while temperature affects the relaxation of steel tendons . For a better understanding on their impact on the post-tensioning loss development, the reader is redirected to Granello et al. (2018a).

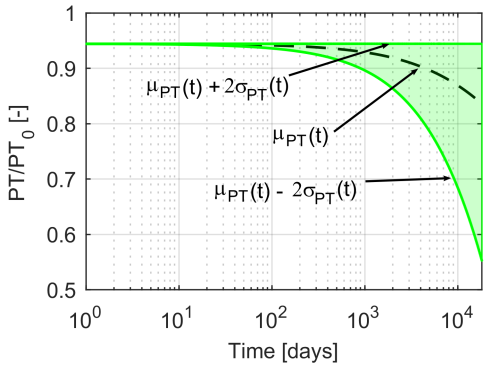

Figure 9. Post-tensioning force over time according to (Granello et al., 2018a). $\mu_{PT}(t)$ average value, $\mu_{PT}(t) + 2\sigma_{PT}(t)$ upper bound and $\mu_{PT}(t) - 2\sigma_{PT}(t)$ lower bound.

The predicted post-tensioning trend over time, $\mu_{PT}(t)$, is reported in Figure 9 and Table 6. It can be noticed that the mean predicted value in 50 years is equal to 16%. The reason for such a 'limited' amount, among other factors such as the use of steel plates in the beam-column

joint, is because the ratio between the post-tensioning steel area A_p over the timber section $A_{\parallel} = A_{\perp}$ is very low. Such scenario is more likely to happen when designing post-tensioned timber frames in high seismic zones, because the members' size is governed by the interstorey drift limit when frequent earthquakes occur.

Table 6. Post-tensioning force evolution over time: $PT_{avg} = \mu_{PT}(t)$ average value, $PT^{-}_{2STD} = \mu_{PT}(t) + 2\sigma_{PT}(t)$ upper bound and $PT^{-}_{2STD} = \mu_{PT}(t) - 2\sigma_{PT}(t)$ lower bound.

Post-tensioning	**Intial**	**10 years**	**25 years**	**50 years**
PT_{avg}	100%	91%	87%	84%
PT^{+}_{2STD}	100%	94%	94%	94%
PT^{-}_{2STD}	100%	82%	70%	55%

When the procedure was used to evaluate the amount of post-tensioning loss of the Trimble building , it provided reasonable results considering the average value of the frames (Granello et al., 2018a). However, if the prediction is compared with each single framel, it is subjected to greater uncertainty due to the intrinsic variability of each frame.

Figure 10 shows the empirical standard deviation of the error (STD) between the prediction and experimental results for the Trimble Navigation Offices. It can be observed that the uncertainty on post-tensioning loss is increasing with time, which can be fairly well captured by Equation (3).

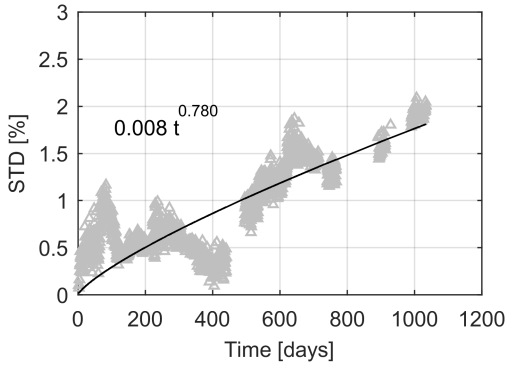

Figure 10. Standard deviation of the error (STD) between the prediction and the data monitored in the Trimble Navigation Offices (Granello et al., 2018a).

In addition to the average losses, Figure 9 and Table 6 report the average value plus (PT^{+}_{2STD}) and minus (PT^{-}_{2STD}) to be two times the standard deviation. Therefore, the green area in Figure 9 represents the possible post-tensioning scenarios within a confidence of 95%, and the average value is represented by the dotted black curve. Note that the initial value is not 100% because

of the inelastic deformation of timber and steel at the moment of stressing, which are assumed to occur instantaneously. This value is also considered as the upper boundary of the prediction, which implies a truncated Gaussian distribution for ε_t.

PERFORMANCE LEVELS

In Figure 11 it is reported the moment-rotation response of the beam-column joint of the specimen with dissipaters. Specifically, the response refers to the joints at the first storey. The performance levels are also highlighted.

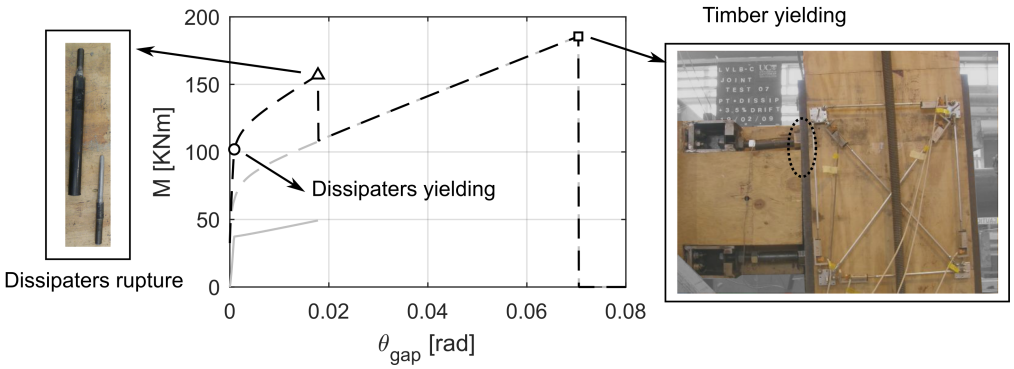

Figure 11. Performance levels for the hybrid rocking connection on the moment-rotation response.

It can be noticed that $PL1_{y,ms}$ occurs almost immediately after the decompression of the joint, for a $\Theta_{gap} = 0.001$. Once the rocking motion is triggered, the dissipaters are activated soon after subjected to yielding.

The dissipaters rupture, i.e., $PL2_{u,ms}$, occurs for approximately $\Theta_{gap} = 0.02$; this value can be controlled during the design phase by modifying the unbonded length of the dissipaters. The current practice (Pampanin et al., 2013) suggests designing dissipaters by having an axial deformation equal to 3% at the ULS, which normally targets a 2.5% drift. The building is designed by following this recommendation, therefore, a gap opening equal to $\Theta_{gap} = 0.02$ occurs after reaching 2.5% drift. Once the dissipaters break, their contribution in terms of moment is set equal to 0.

The timber yielding $PL3_{y,t}$, meaning that the most compressed timber fibers exceed the yielding deformation, occurs at approximately $\Theta_{gap} = 0.07$. In this case, the performance level is reached in the beam because the column is protected by steel plates. However, if the column is not adequately protected by using hardwood or steel, this performance level can be reached

at lower rotations as the strength of timber perpendicular to the grain is significantly lower than the strength of timber parallel to the grain.

When timber locally yields, the inertia of the entire section is reduced causing a degradation of stiffness. This would imply great rotations, and therefore more fibers would be progressively subjected to yielding. A more refined model, using a more detailed approach, should be used to capture this progressive degradation (Valipour et al., 2016). However, it is conservatively assumed that the moment being carried by the connection, after the yielding of timber, is equal to 0.

The moment-rotation analysis was stopped at $\Theta_{gap} = 0.08$. In fact, given this gap opening the building would have an interstorey drift $\Theta_{interstorey}$ greater than 8%. This happens because $\Theta_{interstorey}$ is the sum of gap opening Θ_{gap} and elastic deformation Θ_{el}:

$$\Theta_{interstorey} = \Theta_{el} + \Theta_{gap} \tag{10}$$

Although the New Zealand building code does not specify a drift limitation in terms of collapse limit state, a limit should be introduced to verify the structure against Maximum Credible Earthquakes (MCE) (Hare et al., 2012). In this study, 6% interstorey drift is considered as the collapse limit state.

Because of this assumption, the local performance of the connection has a lack of meaning after 6% interstorey drift. Within this limit, the yielding, or even rupture, of tendons is not occurring. Analyses conducted for different connections have shown that the yielding of tendons always occur at very large interstorey drift (greater than 6%). This is due to timber flexibility: because of the great elastic deformation Θ_{el}, the maximum allowable gap opening Θ_{gap} is limited for a given $\Theta_{interstorey}$.

GROUND MOTIONS SELECTION

The fragility curves were developed by using the multi-stripe method (Baker, 2015). The intensity measure domain was subdivided in "stripes," each one represented by the spectrum given by the New Zealand Standard 1170.5 (2004) for 20, 25, 50, 100, 250, 500, 1000, 2500 years return period, respectively.

For each spectrum (soil category D) representing the seismic hazard, 80 ground motions were selected for the two sites. The ground motions were extracted from the NGA database (Chiou et al., 2008) and scaled with respect to an anchor point in correspondence of the period

$T* = 0.85$s. An example of the spectra and ground motions selected for this study is reported in Figure 12. The spectral values for the different return periods are reported in Table 7.

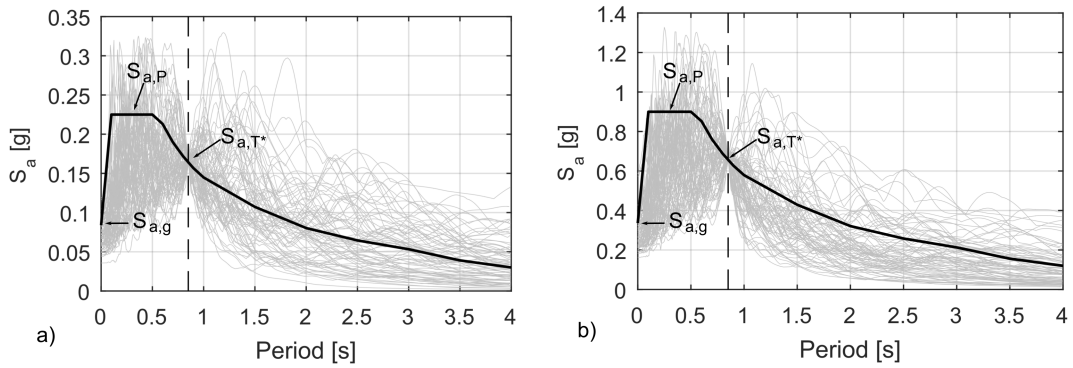

Figure 12. Ground motions spectra for a) 25 and b) 500 years return period in high seismic zone. The spectral acceleration in correspondence of ground $S_{a,g}$, plateau $S_{a,P}$ and anchor point $S_{a,T*}$ is highlighted.

The following conditions were considered during the selection process :

1. the ratio between the spectral acceleration of the original ground motion and the code spectrum in correspondence of the first natural period can not be lower than 0.33 or greater than 3 (New Zealand Standard 1170.5, 2004).

2. the maximum spectral acceleration of the scaled ground motion is not higher than 1.5, which is the maximum spectral acceleration provided by the code.

Both conditions were introduced to avoid:

1. having scaling factors too big or too small which dramatically affect the ground motion intrinsic properties (i.e., a ground motion of low intensity does not have the same frequency content of a ground motion of high intensity (Bradley, 2010));

2. adequately representing the hazard in correspondence of the first natural period as well as the plateau range of periods.

Table 7. Spectra acceleration values in correspondence of the ground $S_{a,g}$, in correspondence of the plateau $S_{a,P}$ and in correspondence of the building period $S_{a,T*}$ for events with different return periods.

Return period (years)	Low seismic zone			High seismic zone		
	$S_{a,g}$ (g)	$S_{a,P}$ (g)	$S_{a,T*}$ (g)	$S_{a,g}$ (g)	$S_{a,P}$ (g)	$S_{a,T*}$ (g)
20	0.04032	0.1080	0.0752	0.0672	0.1800	0.1254
25	0.0504	0.1350	0.0941	0.0840	0.2250	0.1568
50	0.0706	0.1890	0.1317	0.1176	0.3150	0.2195
100	0.1009	0.2700	0.1881	0.1680	0.4500	0.3135
250	0.1512	0.4050	0.2822	0.2520	0.6750	0.4703
500	0.2016	0.5400	0.3762	0.3360	0.9000	0.6270
1000	0.2621	0.7020	0.4891	0.4368	1.170	0.8151
2500	0.3629	0.9720	0.6772	0.6048	1.620	1.129

RESULTS

PARAMETERS OVER TIME

The parameters α and β describing the fragility curves were calculated for 10 levels of post-tensioning loss, i.e., 0%, 5%, 10%, 15%, 20%, 25%, 30%, 35%, 40%, and 45% [c)].

In this study we impose the scaling parameter β for a specific performance level to be constant across the different PT levels. Imposing a constant β avoids intersection between the fragility curves, which are merely due to "jumps" of β values, due to the classification of EDP points on the onset of a limit state threshold.

Therefore, an average beta β_{avg} is estimated for each curve associated with a specific performance level, and the location parameter, α, is recomputed on the reduced parameter space. This corresponds to the engineering assumption that the reliability of the structural system is uniformly decreasing (across all IM values) with the post tension losses.

The values of β is reported in Figure 13a and 13b for the building without and with supplemental damping, respectively. The continuous line in both figures shows the average value β_{avg}, which is also reported in Table 8.

The values of α are reported in Figure 14 for the two buildings, without and with supple-

[c)] The levels were selected based on Figure 9

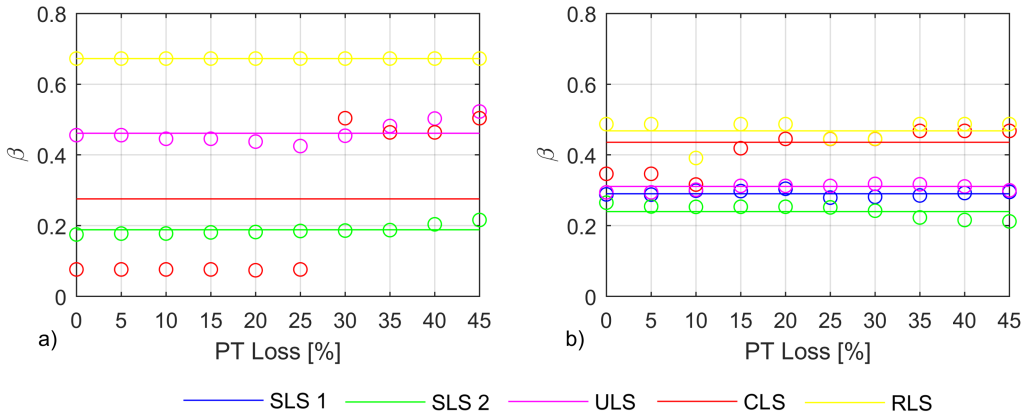

Figure 13. Variance β for the building a) without and b) with supplemental damping.

Table 8. Values of β_{avg} and $\alpha = a'x + a_0$, where x is the amount of post-tensioning loss.

	Without dissipaters				**With dissipaters**				
	SLS 2	**ULS**	**CLS**	**RLS**	**SLS 1**	**SLS 2**	**ULS**	**CLS**	**RLS**
β_{avg}	0.188	0.461	0.276	0.672	0.290	0.240	0.311	0.436	0.468
a'	-0.00065	-0.0020	-0.0046	-0.55	-0.00041	-0.00015	-0.0013	-0.0031	-0.0012
a_0	0.170	0.896	1.43	60.7	0.133	0.216	1.27	1.95	2.38

mental damping. Results were interpolated with the following linear model:

$$\alpha(PT) = a'PT + a_0 \tag{11}$$

which values are reported in Table 8.

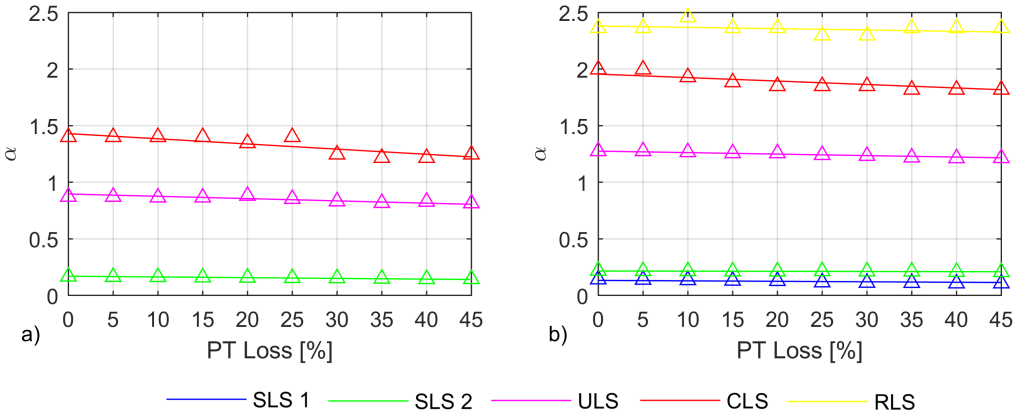

Figure 14. Average α for the building a) without and b) with supplemental damping.

It can be noticed from Figure 14 that post-tensioning loss has an impact on the fragility

curves. The greater the post-tensioning loss, a lower value of α occurs. This means that, generally speaking, for a given intensity measure, the probability of overcoming a specific performance level increases while losses increase.

Note that the values of α for the RLS in the building without additional damping (yellow triangles in Figure 14) are not even present because out of scale. These values are in fact 10 times greater than the CLS, which means the probability of overcoming re-centering is 10 times lower in average than the probability of reaching 6% drift. This was expected because the building does not have dissipaters, and the re-centering ratio is equal to 1 and does not depend on the post-tensioning level. Also, it has to be noted that the α related to re-centering is higher than the α related to collapse. This means that the probability of re-centering is always higher than the probability of collapse.

By substituting Equation 2 into the Equation 11, the expression of α values can be obtained as

$$A_t = a' \cdot (\mu_{PT}(t) + \varepsilon_t) + a_0 \tag{12}$$

In Figure 15, the values of α for the building without additional damping are reported. The dotted line represents the response over time of the mean, $\mu_{A_t} = a'\mu_{PT}(t) + a_0$, while the boundaries represent the response considering 2 times the standard deviation $\pm 2\sigma_{A_t}$ dependent on the post-tensioning loss uncertainty. In the same way, the values of A_t for the building with additional dissipaters are reported in Figure 16.

FAMILY OF FRAGILITY CURVES

The time variant fragility including the PT uncertainty is given by Equation (15):

$$P(D = d|im, \boldsymbol{\Theta}_{f,t} = \boldsymbol{\theta}_f) = \Phi\left(\frac{\ln(im/\alpha)}{\beta}\middle| A_t = \alpha, B_t = \beta_{avg}\right). \tag{13}$$

Then, the mean plug-gin approximation over time can be obtained as:

$$P(D = d|im, \boldsymbol{\Theta}_{f,t} = \bar{\boldsymbol{\theta}}_f) = \Phi\left(\frac{\ln\left(im/(a'\mu_{PT}(t) + a_0)\right)}{\beta_{avg}}\right), \tag{14}$$

and the 2STD plug-gin approximation over time can be obtain as

$$P(D = d|im, \boldsymbol{\Theta}_{f,t} = \boldsymbol{\theta}_{f,\pm 2\sigma}) = \Phi\left(\frac{\ln\left(im/\left(a'(\mu_{PT}(t) \pm 2\sigma_{PT}(t)) + a_0\right)\right)}{\beta_{avg}}\right). \tag{15}$$

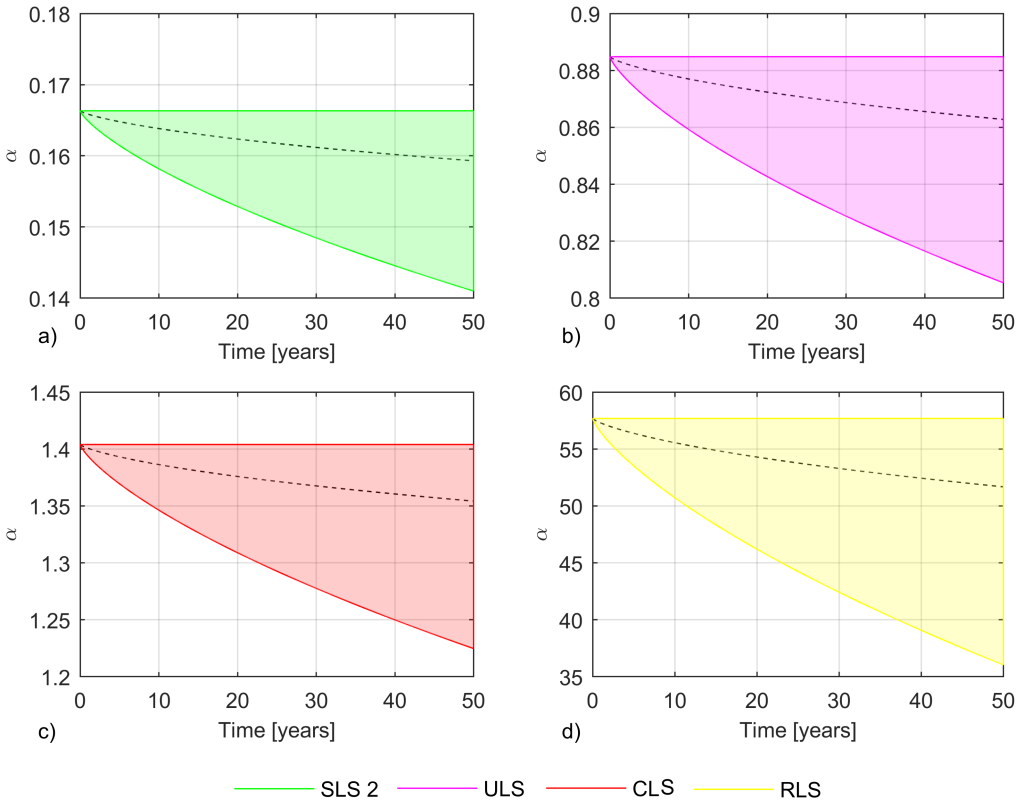

Figure 15. Parameter α over time for each performance level in the building without supplemental damping (black line= mean value μ, boundaries = $\mu \pm 2\sigma$.)

Observe that these fragility functions are *marginal* fragility, i.e., they do not include the correlation between different instants of time. It is considered out of the current scope of this study to provide the definition of such time-correlation models mainly because a correlation analysis is not available. Moreover, no inspections or measurements, which will justify updating the model after information becomes available, are included in the design. In this case a full Gaussian process, which includes a correlation model between different instants of time, can be integrated in the current model. Observe that in this case the current formulations of A_t and B_t play the role of "prior information."

Furthermore, if only one fragility is desired (instead of a family of fragility) which also includes the PT uncertainty, Equation 16 can be used:

$$P(D = d|im, \boldsymbol{\Theta}_{f,t} = \boldsymbol{\theta}_f) = \int_{\alpha} \Phi\left(\frac{\ln(im/\alpha)}{\beta}\middle|\alpha, \beta_{avg}\right) f(\alpha|t)d\alpha. \tag{16}$$

The fragility curves at the initial time for the building with dissipaters are reported in Figure 17a. It can be noticed that the building has less than 20% probability to damage the no-structural

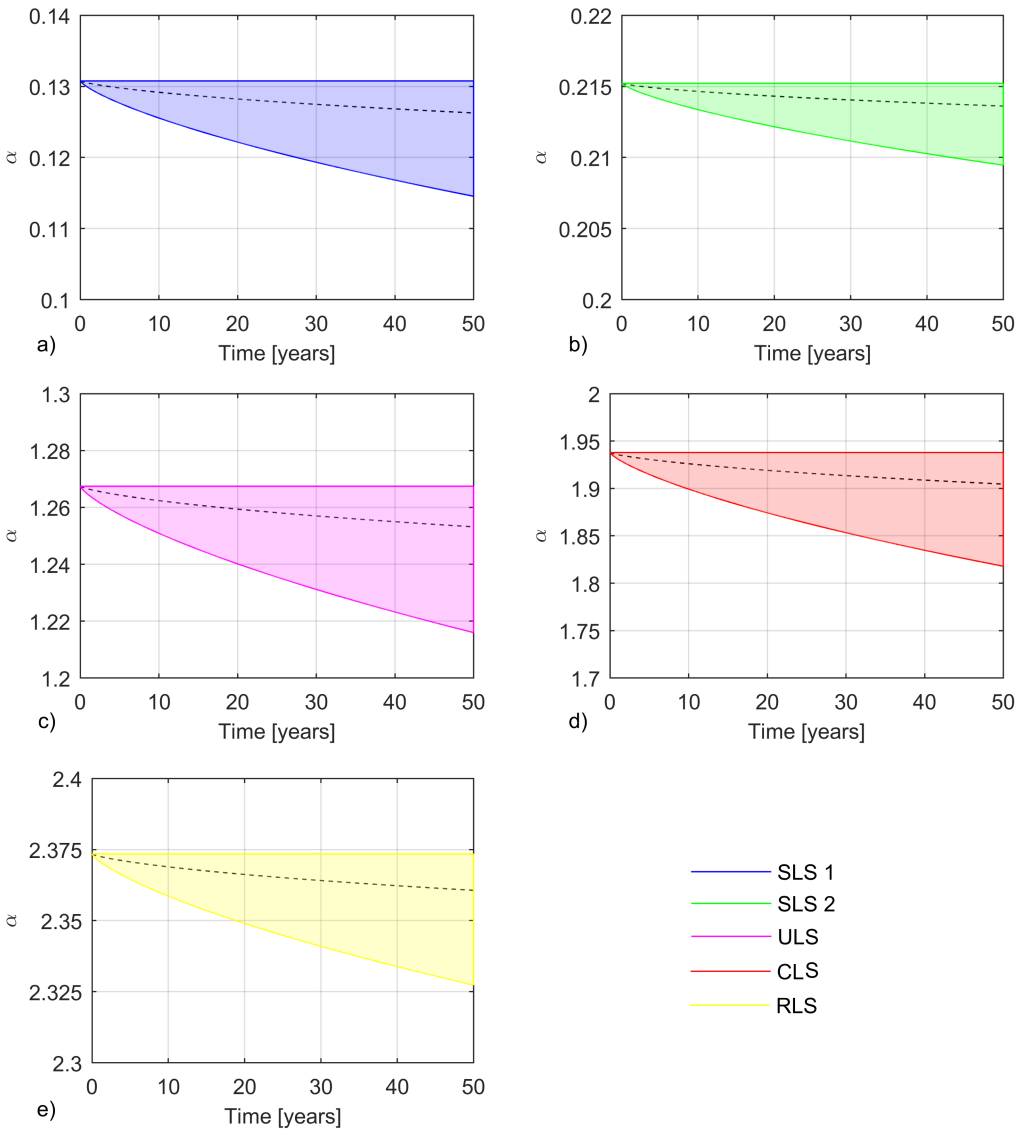

Figure 16. Parameter α over time for each performance level in the building with supplemental damping (black line= mean value μ_{A_t}, boundaries = $\mu_{A_t} \pm 2\sigma_{A_t}$).

elements (SLS2) for a seismic event with a return period equal to 25 years, and a considerably small probability (i.e. 0.01%) to damage to the structural elements (ULS) by an event with return period equal to 500 years. Furthermore, there is less than 16% probability to exceed a 6% drift (CLS) under an event with a return period equal to 2500 years.

In terms of re-centering, the building shows a probability greater than 99.9% to have residual deformation smaller than 0.5% drift for events with a return period lower than 500 years. Furthermore, there is 70% probability that the dissipaters are subjected to yielding for an event with a return period equal to 25 years.

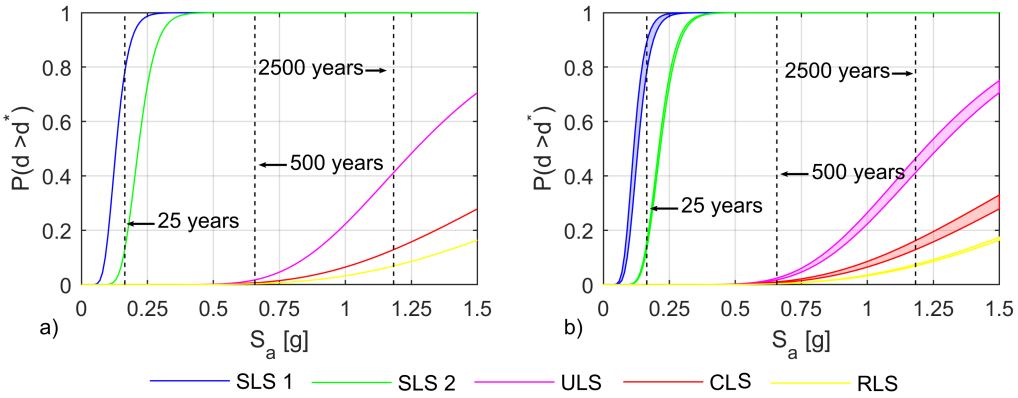

Figure 17. Fragility curves for the building with dissipaters at A) initial time and B) after 50 years.

Figure 17b reports the family of fragility curves at 50 years. The lower bound is represented by a scenario with post-tensioning loss equal to 45% (i.e., the expected average value minus 2 standard deviations). Results shows that the performance at SLS2, ULS, CLS and RLS is similar to the initial one. However, the probability of yielding the dissipaters increases from 70% to almost 100% for an event with a 25 years return period.

Dissipaters are in fact earlier activated when post-tensioning loss occurs, because the clamping force between the beam and the column is reduced. Therefore, they start dissipating energy at lower level of drift. Because of this, the interstorey drift does not significantly increase, although the connection capacity is reduced.

However, they are activated more often during the building life, as an event with a lower return period can easily trigger the rocking motion. If dissipaters are external (e.g., in the beam-column joint case), the cost is minor due to the easy access and process. However, if dissipaters are internal (e.g., column-foundation case) the replacement might take more time with a consequently higher cost replacement.

Figure 18a reports the fragility curves for the building without dissipaters at initial time. It can be noticed the specimen shows approximately 1% probability of damaging the no-structural elements for an event with a 25 years return period; approximately 5% probability of damaging the structural elements for an event with 500 years return period; and less than 5% probability of overcoming 6% drift for an event with a 2500 years return period. Furthermore, the building shows more than 99,9% probability of having a residual interstorey drift lower than 0.5% for all the events with a return period below 2500 years.

Generally speaking, it can be seen from Figure 18b that the area enclosed between the SLS,

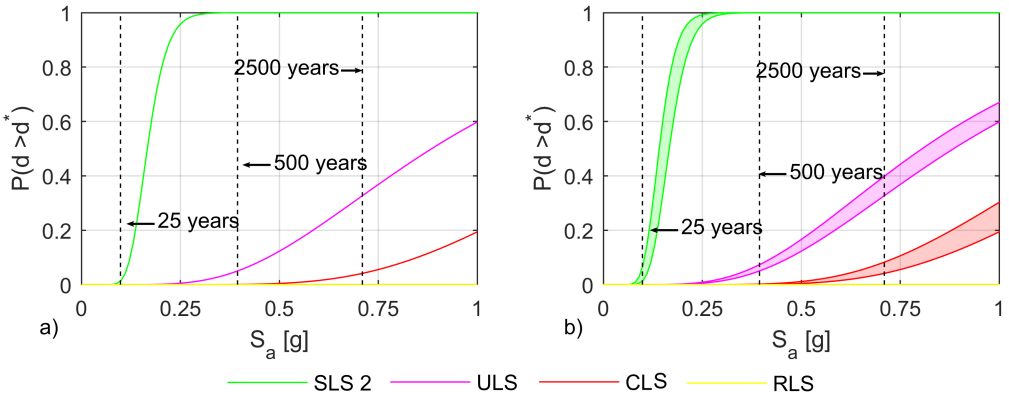

Figure 18. Fragility curves for the building without dissipaters at A) initial time and B) after 50 years.

ULS and CLS curves at initial time and the same curves at 50 years, is greater in respect to the case of the building with additional damping. This means that post-tensioning losses have a greater impact when no dissipaters are provided, and the consequent shift of the fragility curve at 50 years is higher (with respect to the building with additional dissipaters).

When looking at design code provisions, the probability of exceeding the SLS, ULS and CLS limit state for specific events with a 25, 500 and 2500 years return period, rises approximately to 7%, 7% and 8% , respectively. This means that the building still shows an acceptable code compliant behavior after 50 years. However, from the pure seismic performance point of view, the greater shift in the fragility curves over time proves that dissipaters mitigate the effect of post-tensioning loss in terms of overall damage.

In terms of re-centring, the building with no dissipaters after 50 years still maintains a probability of exceeding the RLS lower than 0.1% an event with return period lower than 2500 years. This again is due to the fact that, if dissipaters are not provided, the only post-tensioned joint is able to re-center although losses occur.

CONCLUSIONS

The paper presented a methodology to evaluate the impact of post-tension losses on the seismic performance of post-tensioned timber frame buildings. The methodology is based on developing a fragility analysis which parameters are time dependent to take into account the development and uncertainty of post-tensioning losses.

The post-tensioning force over time was predicted by using an equation from literature,

while the uncertainty in the prediction was identified by using data monitored on an operative building. Furthermore, a set of performance levels specifically for post-tensioned timber rocking structures was introduced.

The method was then applied to two Pres-Lam frame buildings, which were designed respectively in a high seismic hazard zone (corresponding to a maximum spectral acceleration in correspondence of the plateau equal to 0.9 g for a 500 years return event) and a low seismic hazard zone (corresponding to maximum spectral acceleration in correspondence of the plateau equal to 0.54 g for a 500 years return event). The building in the high seismic zone was designed by combining unbonded post-tensioned tendons with dissipaters, while the building in the low seismic zone relies only on unbonded post-tensioned tendons.

In the cases analysed, results show that post-tensioning losses have minor on the seismic performance when looking at the high magnitude earthquakes. If dissipaters are provided, they further mitigate the effect of post-tensioning losses. However, the reduction of post-tensioning affects the building performance for lower level of earthquakes prematurely activating the rocking motion.

Further buildings typologies should be investigated to fully understand the influence of post-tensioning loss. However, the fragility based methodology proposed can be used as a powerful tool for assessing the time-dependent seismic performance of these type of structures.

REFERENCES

1170.0, N., 2002. *New Zealand Standard*. New Zealand.

Baker, J. W., 2015. Efficient analytical fragility function fitting using dynamic structural analysis. *Earthquake Spectra* **31**, 579–599.

Bradley, B. A., 2010. A generalized conditional intensity measure approach and holistic ground-motion selection. *Earthquake Engineering & Structural Dynamics* **39**, 1321–1342.

Brown, A., Lester, J., Pampanin, S., and Pietra, D., 2012. Rebuilding timber navigations offices using a damage-limiting seismic system. In *World Conference on Timber Engineering, Quebec City*.

Chiorino, M., Napoli, P., Mola, F., and Koprna, M., 1984. Structural effects of time-dependent behaviour of concrete. *CEB Bull. No. 142/142 Bis* .

Chiou, B., Darragh, R., Gregor, N., and Silva, W., 2008. NGA project strong-motion database. *Earthquake Spectra* **24**, 23–44.

Christopoulos, C., Filiatrault, A., Uang, C., and Folz, B., 2002. Post-Tensioned Energy Dissipating Connections for Moment Resisting Steel Frames. *Journal of Structural Engineering* **128**, 1111–1120.

Comite Europeen de, N., 2005. *Eurocode 8 - Design of structures for earthquake resistance.* Brussels, Belgium.

Curtain, B., Dekker, D., Chung, S., and Palermo, A., 2012. Design of Carterton Event Centre: An

example of innovative collaboration between architecture and timber engineering. In *Proceedings of the 12th World Conference on Timber Engineering WCTE, Auckland, New Zealand*.

Davies, M. and Fragiacomo, M., 2011. Long-term behavior of prestressed LVL members. I: Experimental tests. *Journal of Structural Engineering* **137**, 1553–1561.

Di Cesare, A., Ponzo, F. C., Nigro, D., Pampanin, S., and Smith, T., 2017. Shaking table testing of post-tensioned timber frame building with passive energy dissipation systems. *Bulletin of Earthquake Engineering* **15**, 4475–4498. doi:10.1007/s10518-017-0115-9.

FEMA, P., 2009. 695. Quantification of Building Seismic Performance Factors. *Federal Emergency Management Agency* .

Fragiacomo, M. and Davies, M., 2011. Long-term behavior of prestressed LVL members. II: Analytical approach. *Journal of Structural Engineering* **137**, 1562–1572.

Granello, G., Leyder, C., Palermo, A., Frangi, A., and Pampanin, S., 2018a. Design Approach to Predict Post-tensioning Losses in Post-tensioned Timber Frames. *Journal of Structural Engineering* **Accepted**. doi:10.1061/(ASCE)ST.1943-541X.0002101.

Granello, G., Palermo, A., Pampanin, S., Smith, T., and Sarti, F., 2018b. The Implications of Post-Tensioning Losses on the Seismic Response of Pres-Lam Frames. *Bulletin of New Zealand Society for Earthquake Engineering* **51**, 57–69.

Hare, J., Oliver, S., and Galloway, B., 2012. Performance Objectives for Low Damage Seismic Design of Buildings. In *NZSEE conference, Christchurch*.

Holden, T., Devereux, C., Haydon, S., Buchanan, A., and Pampanin, S., 2016. NMIT Arts & Media BuildingInnovative structural design of a three storey post-tensioned timber building. *Case Studies in Structural Engineering* **6**, 76–83.

Leyder, C., Wanninger, F., Frangi, A., and Chatzi, E., 2015. Dynamic response of an innovative hybrid structure in hardwood. *Proceedings of the Institution of Civil Engineers-Construction Materials* **168**, 132–143.

Marriott, D., Pampanin, S., and Palermo, A., 2009. Quasi-static and pseudo-dynamic testing of unbonded post-tensioned rocking bridge piers with external replaceable dissipaters. *Earthquake engineering & structural dynamics* **38**, 331–354.

McCormick, J., Aburano, H., Ikenaga, M., and Nakashima, M., 2008. Permissible residual deformation levels for building structures considering both safety and human elements. In *Proceedings of the 14th world conference on earthquake engineering*, pp. 12–17.

Moroder, D., Smith, T., Dunbar, A., Pampanin, S., and Buchanan, A., 2018. Seismic testing of post-tensioned Pres-Lam core walls using cross laminated timber. *Engineering Structures* .

New Zealand Standard 1170.1, N., 1993. *New Zealand Standard*. New Zealand.

New Zealand Standard 1170.5, N., 2004. *New Zealand Standard*. New Zealand.

Newcombe, M., Pampanin, S., Buchanan, A., and Palermo, A., 2008. Section analysis and cyclic behavior of post-tensioned jointed ductile connections for multi-story timber buildings. *Journal of Earthquake Engineering* **12**, 83–110.

Palermo, A., 2004. The use of controlled rocking in the seismic design of bridges. *Doctate Thesis, Technical Institute of Milan, Milan* .

Palermo, A., Pampanin, S., Buchanan, A., and Newcombe, M., 2005. Seismic design of multi-storey buildings using laminated veneer lumber (LVL). In *New Zealand Society for Earthquake Engineering Conference*. Wairakei, New Zealand.

Pampanin, S., Palermo, A., and Buchanan, A. H., 2013. Design Guide Australia and New Zealand:

574 Post-Tensioned Timber Buildings. *Expan Design Guides* .

575 Pampanin, S., Priestley, M. N., and Sritharan, S., 2001. Analytical modelling of the seismic behaviour
576 of precast concrete frames designed with ductile connections. *Journal of Earthquake Engineering* **5**,
577 329–367.

578 Ponzo, F. C., Di Cesare, A., Lamarucciola, N., Nigro, D., and Pampanin, S., 2017. Modelling Of Post-
579 tensioned Timber-framed Buildings With Seismic Rocking Mechanism At The Column-foundation
580 Connections. *International Journal of Computational Methods and Experimental Measurements* **5**,
581 966–978.

582 Porter, K., 2015. Beginner?s guide to fragility, vulnerability, and risk. *Encyclopedia of Earthquake*
583 *Engineering* pp. 235–260.

584 Priestley, M., 2000. Performance based seismic design. *Bulletin of the New Zealand society for earth-*
585 *quake engineering* **33**, 325–346.

586 Priestley, M., Calvi, G., and Kowalsky, M., 2007. Displacement-based seismic design of structures.
587 *IUSS Press* .

588 Priestley, N. M. J., 1991. Overview of the PRESSS Research Program. *PCI Journal* **36**, 50–57.

589 Sarti, F., Palermo, A., and Pampanin, S., 2015. Quasi-static cyclic testing of two-thirds scale unbonded
590 posttensioned rocking dissipative timber walls. *Journal of Structural Engineering* **142**, E4015005.

591 Sarti, F., Palermo, A., and Pampanin, S., 2016. Fuse-Type External Replaceable Dissipaters: Experi-
592 mental Program and Numerical Modeling. *Journal of Structural Engineering* **142**, 04016134.

593 Sarti, F., Palermo, A., Pampanin, S., and Berman, J., 2017a. Determination of the seismic performance
594 factors for posttensioned rocking timber wall systems. *Earthquake Engineering & Structural Dynam-*
595 *ics* **46**, 181–200. doi:10.1002/eqe.2784.

596 Sarti, F., Smith, T., Danzig, I., and Karsh, E., 2017b. Pres-Lam in the US: the seismic design of the Peavy
597 Building at Oregon State University. In *New Zealand Society of Structural Engineers Conference*.
598 Wellington, New Zealand.

599 Shinozuka, M., Feng, M. Q., Lee, J., and Naganuma, T., 2000. Statistical analysis of fragility curves.
600 *Journal of engineering mechanics* **126**, 1224–1231.

601 Smith, T., 2014. *Post-tensioned Timber Frames with Supplemental Damping Devices*. PhD Thesis,
602 University of Canterbury, Christchurch, New Zealand.

603 Smith, T., Ponzo, F. C., Di Cesare, A., Pampanin, S., Carradine, D., Buchanan, A. H., and Nigro,
604 D., 2014. Post-tensioned glulam beam-column joints with advanced damping systems: Testing and
605 numerical analysis. *Journal of Earthquake Engineering* **18**, 147–167.

606 Valipour, H., Khorsandnia, N., Crews, K., and Palermo, A., 2016. Numerical modelling of
607 timber/timber–concrete composite frames with ductile jointed connection. *Advances in Structural*
608 *Engineering* **19**, 299–313.

609 Wanninger, F. and Frangi, A., 2014. Experimental and analytical analysis of a post-tensioned timber
610 connection under gravity loads. *Engineering structures* **70**, 117–129.

611 Wanninger, F., Frangi, A., and Fragiacomo, M., 2014. Long-Term Behavior of Posttensioned Timber
612 Connections. *Journal of Structural Engineering* pp. DOI: 10.1061/(ASCE)ST.1943–541X.0001121.
613 doi:10.1061/(ASCE)ST.1943-541X.0001121.